Nanoscale

PAPER

View Article Online
View Journal | View Issue

Cite this: *Nanoscale*, 2019, **11**, 1351

Realization of an efficient electron source by ultraviolet-light-assisted field emission from a one-dimensional ZnO nanorods/n-GaN heterostructure photoconductive detector†

Yiren Chen, ‡[a] Zhiwei Zhang,[a] Hong Jiang,[a] Zhiming Li,[a] Guoqing Miao,[a] Hang Song,*[a] Liqin Hu‡[b] and Tailiang Guo*[b]

Field emission electron beam (EB) pumped AlGaN-based semiconductors are considered to be a potentially promising way to overcome the technical bottlenecks that restrict the development of AlGaN-based UV luminescence devices and realize efficient UV light sources. However, the required field emission electron sources based on nanomaterials are still inefficient due to their low field emission current density. Herein, a type of UV-light-assisted self-positive-feedback enhanced field emission electron source is proposed to develop a high-efficiency electron source which is promising for application in EB pumped AlGaN-based UV light sources that can also be generalized to deep UV (DUV) luminescence devices. The UV-light-assisted field emission source is composed of an n-GaN metal–semiconductor–metal (MSM) structure photodetector assembled with 1D ZnO nanorods by a self-assembled hydrothermal growth method, which simultaneously possesses attributes of the photoelectric effect and electron emission. The optical, photoelectric, and field emission properties are investigated in detail. The results show that the 1D ZnO nanorods/n-GaN heterostructure photodetector presents an obvious photoconductive effect. It has a peak spectral responsivity of 0.793 A W^{-1} at a bias voltage of 1.3 V, corresponding to an EQE higher than 267.8%, with an internal photoconductive gain reaching up to 2.51×10^3. As to the field emission properties, its turn-on electric field can be greatly reduced from 3.6 V μm^{-1} in the dark to 1.36 V μm^{-1} under UV illumination, and the field emission current density increases from lower than 3 mA cm^{-2} to as high as 8 mA cm^{-2} at an electric field of 4.5 V μm^{-1}. The mechanism involved can be attributed to an increase of electron concentration in both the conduction bands and an increase of conduction band bending under UV illumination that reduces the effective potential barrier height of the ZnO nanorods. Through this research, an efficient field emission electron source with a self-enhancing effect is developed by combining the photoelectric effect with the electron emission process.

Received 9th October 2018,
Accepted 17th December 2018

DOI: 10.1039/c8nr08154a

rsc.li/nanoscale

Introduction

In the face of the enormous ecological and economic benefits of AlGaN-based ultraviolet (UV) light sources, overcoming the low external quantum efficiency (EQE) caused by the intrinsically low hole concentrations in p-type AlGaN is urgently required. Thus, the electron-beam (EB) pumped method using a structure similar to a field emission display is proposed as a promising alternative, which has the following advantages: (i) the pumping object (so-called target materials) is unrestrained and can be a single layer of the intrinsic or doped material, or a low-dimensional structure material such as single or multiple quantum well (QW) and superlattices; (ii) the effective depth of interaction under high-energy electron beam bombardment is large and the output light power can be improved by increasing the thickness of the active target. With growing interest over EB pumped AlGaN-based UV light sources, it leverages the important application potential of compact and efficient electron sources.[1,2] Electron sources based on field emission, which have been extensively applied in both vacuum optoelectronic and microelectronic devices, such as field emission displays, X-ray generators, microwave power amplifiers, and terahertz generators,[3–6] thus provide a

[a]*State Key Laboratory of Luminescence and Applications, Changchun Institute of Optics, Fine Mechanics and Physics, Chinese Academy of Sciences, Changchun 130033, People's Republic of China. E-mail: songh@ciomp.ac.cn*
[b]*Institute of Optoelectronic Technology, Fuzhou University, Fuzhou 350002, People's Republic of China. E-mail: gtl_fzu@hotmail.com*

†Electronic supplementary information (ESI) available. See DOI: 10.1039/c8nr08154a

‡These authors contributed equally.

good choice. At the same time, higher requirements are put forward to the performance of the electron sources based on field emission.

As a key part of a field emission electron source, the field emitter is of great importance. Among the different types of field emitters, low-dimensional nanostructured zinc oxide (ZnO), as a direct wide bandgap semiconductor material sensitive to the ultraviolet light, has the richest variety of different nanostructures with one- (1D), two- (2D), and three-dimensional (3D) morphologies, and is considered to be among the most promising materials for nanoscale electronic and optoelectronic devices.[4,7–9] As a representative of the 1D structure, ZnO nanorods (NRs) have been widely used in a range of fields, such as light-emitting diodes (LEDs),[10,11] dye-sensitized solar cells,[12,13] laser diodes (LDs),[14,15] field effect transistors (FETs),[16] ultraviolet photodetectors (UV-PDs),[17–19] gas sensors,[20] and so on. What is more remarkable, due to their high aspect ratios, nanoscale tips, controllable size, and directional growth on hetero-semiconductors, ZnO nanorods have drawn great attention for application as a cold cathode in field-emission-based devices. However, so far the field emission current density based on the ZnO nanorod cathodes is still low, which hinders their practical application as an electron beam pumping source to excite semiconductor targets. Surface treatment such as sharpening the ZnO nanorods or decorating them with metallic nanoparticles and graphene oxide, and doping in ZnO nanorods with group III or IV elements have been investigated in order to improve their field emission current density.[21–24]

In this work, for the purpose of improving the field emission current density based on 1D ZnO nanorods, a photo-assisted modulation method is proposed. A 1D ZnO nanorods/n-GaN heterostructure photoconductive detector is prepared by the self-assembled hydrothermal growth of 1D ZnO nanorods on a metal–semiconductor–metal (MSM) structure n-GaN photodetector, which can act as an ultraviolet-light-assisted enhanced field emission electron source. The related photoelectric and field-emission properties were investigated in detail. The results show that the field emission properties of the 1D ZnO nanorods/n-GaN heterostructure photoconductive detectors are effectively enhanced, and the mechanism involved is also clarified. The study on the ultraviolet-light-assisted enhanced field emission electron source is beneficial to developing a type of optical field positive-feedback enhanced field emission electron beam pumped UV or deep UV light source.

Experimental section

Epitaxial growth of the n-GaN material

The n-GaN epilayer was epitaxially grown on a 2-inch double polished *c*-plane sapphire substrate by metal–organic chemical vapour deposition (MOCVD). In the growth process, trimethylgallium (TMGa) and ammonia (NH_3) were used as Ga and N precursors, respectively, while silane (SiH_4) was used as the n-type dopant. Hydrogen (H_2) was used as the carrier gas. Prior to growth, the surface of the sapphire was thermally desorbed at 1100 °C under H_2 for 10 min. Then, a 30 nm-thick low-temperature GaN (LT-GaN) nucleation layer was grown on the sapphire substrate at 550 °C followed by a 1 μm-thick high-temperature GaN (HT-GaN) undoped epilayer and a 500 nm-thick Si-doped GaN (n-GaN) layer grown at 1050 °C. The electron carrier concentration and the mobility of the n-GaN were measured to be 5.8×10^{18} cm^{-3} and 110 cm^2 $(V\ s)^{-1}$, respectively.

Fabrication of MSM structure n-GaN photodetectors

In the process of fabricating the MSM structure photodetectors based on n-GaN, Ti/Al/Ni (30 nm/200 nm/300 nm) multilayer interdigital electrodes were firstly deposited by electron-beam evaporation assisted by standard photolithography and lift-off processes.[25] The dimensions of the finger electrodes were 100 μm long and 7 μm wide with a spacing of 8 μm. Then, the photodetectors were rapidly thermally annealed in a N_2 atmosphere at 450 °C for 120 s, to realize a good ohmic contact.

In situ assembling 1D ZnO nanorods on a MSM structure n-GaN photodetector

The aqueous solution growth method was adopted to *in situ* assemble 1D ZnO nanorods on the MSM structure n-GaN photodetector. Prior to growth, the surface of the n-GaN film between the interdigital electrodes underwent degreasing treatment in isopropyl alcohol solution for 3 min. Then, the MSM structure n-GaN photodetector was rinsed by deionized water. Subsequently, it was soaked in a 20 mM $Zn(NO_3)_2$/hexamethylenetetramine (HMT) aqueous solution for 72 h. Finally, the growth of 1D ZnO nanorods was performed in a mixed solution at a constant temperature of 100 °C for 10 h.

Characterization and measurement

The carrier concentration and the mobility of the n-GaN epilayer were evaluated by a Hall effect measurement system (Lake Shore, 8400 Series HMS). The surface morphology of the MSM structured n-GaN photodetector with and without the assembled 1D ZnO nanorods were characterized by field emission scanning electron microscope (SEM, Hitachi S4800). In order to differentiate ZnO and n-GaN qualitatively, energy dispersive X-ray spectroscopy (EDS, Genesis 2000) was used. The crystalline properties of the materials were evaluated by a high-resolution X-ray diffractometer (HRXRD, Bruker D8) with a Cu $K\alpha_1$ radiation (λ = 1.5406 Å), mainly using the 2θ–ω scan pattern and reciprocal space mapping (RSM) around the (0002) and $(10\bar{1}5)$ reflections. The spectral responsivity and the corresponding external quantum efficiency (EQE) for the photodetectors were measured by an ultraviolet spectral response test system, which consisted of a xenon lamp as the light source, a chopper, a monochromator, a lock-in amplifier, and a calibrated silicon photodetector as the standard reference.[26] The PL spectra were measured by a spectrophotometer with a 50 mW 213 nm-wavelength Nd:YAG deep UV laser as the excitation source. The transient spectral response of the

photodetector was stimulated by a 10 mW 365 nm-wavelength Nd:YAG UV laser and recorded with a digital oscilloscope (Tektronix DPO 5104). The current–voltage (I–V) characteristics of the photodetector in the dark and under UV illumination were measured with a semiconductor parameter analyzer (Agilent B1500A). The field emission current density *vs.* electric field (J–E) curves and the time-resolved field emission current density to pulsed UV light were acquired by a field emission test system equipped with one Agilent 34401A source meter as the ammeter and the other as the voltmeter.[27] It should be noted that, the field emission performances in the paper are conducted with a diode structure device without any accelerating pole or any focusing pole.

Results and discussion

Fig. 1(a) and (b) show the SEM images of the as-fabricated and after *in situ* assembled 1D ZnO nanorods MSM structure n-GaN photodetector. The dimensions of the interdigitated electrodes are described in the Experimental section. The inset of Fig. 1(a) shows the schematic diagram of the as-fabricated MSM structured n-GaN photodetector. After *in situ* self-assembled solution growth of 1D ZnO nanorods, the 1D ZnO nanorods/n-GaN heterostructure photodetector is presented in Fig. 1(b). The corresponding schematic diagram and partial enlargement diagram are shown in the inset of Fig. 1(b) and (c), respectively. As can be seen, the n-GaN film between the interdigital electrodes is grown by self-assembly of a large number of 1D ZnO nanorods with a diameter of about 100 nm.

In order to qualitatively analyze the element composition, EDS patterns for the 1D ZnO nanorods/n-GaN sample at different positions are measured. As shown in the inset of Fig. 2(a), two test locations are marked with a black letter a and a red letter b, respectively. The corresponding EDS patterns for location a and b are presented in Fig. 2(a), in which the elements of N, O, Zn, Ga and Si can be observed. Among them, a high atomic percent (at%) of Zn and O in black curve indicates the main material at location a is ZnO nanorods while a high at% of Ga and N in the red curve indicates the main material at location b is GaN.

To further investigate the crystalline characteristics of the 1D ZnO nanorods/n-GaN heterogeneous structural materials, the symmetrical RSM around the (0002) reflection and the asymmetrical RSM around the $(10\bar{1}5)$ reflection are measured by HRXRD, as shown in Fig. 2(b) and (c), respectively. As a contrast, the symmetrical RSM around the (0002) reflection and the asymmetrical RSM around the $(10\bar{1}5)$ reflection for as-grown n-GaN epilayer are also demonstrated, both of which are presented in Fig. S1 of ESI.† Their related 2θ–ω scanning curves are inserted in Fig. S1(a) and (b),† respectively. As seen in Fig. S1(a),† the RSM around the (0002) reflection for the n-GaN epilayer consists of a well-resolved main peak located at $2\theta_{(0002)} = 34.56°$, as emphasized in the inset (0002) plane 2θ–ω scanning curve, an ellipsoidal shaped broadening reciprocal space points (RLPs) and sharp specular intensity sections. The broadening of the RLPs in the ω-scan direction results from the finite lateral coherence length and the tilt of the mosaic blocks.[28,29] The sharp specular intensity sections along the $2\theta/\omega$-scan direction can be traced over a large angular region, which closely relate to the highly ordered GaN crystal on a long scale along the c-axis.[28,30,31] In the asymmetrical RSM around the $(10\bar{1}5)$ reflection (Fig. S1(b)†), a well-resolved main peak located at $2\theta_{(10\bar{1}5)} = 104.98°$ surrounded by a series of contour lines (described by colors) are presented. The tilt and the lateral coherence length of the mosaic blocks broaden the RLPs of n-GaN epilayer along both the ω-scan and $2\theta/\omega$-scan directions. The a and c lattice parameters of n-GaN can be calculated from Bragg's law and the interplanar spacing equation for hexagonal crystals given by[30,32]

$$2d_{hkl} \cdot \sin\theta_{hkl} = n\lambda \quad (1)$$

$$\frac{1}{d_{hkl}^2} = \frac{4(h^2 + hk + k^2)}{3a^2} + \frac{l^2}{c^2} \quad (2)$$

where h, k, and l are the Miller indices of the diffraction plane. n is the diffraction order. λ is the wavelength of the Cu $K\alpha_1$ radiation. d_{hkl} and θ_{hkl} are on behalf of the interplanar spacing and the scattering angle of the (hkl) plane, respectively. In this paper, the a and c lattice parameters of the as-grown n-GaN are calculated to be 0.31893 nm and 0.51865 nm from a symmetrical reflection, *viz.* (002) plane and an asymmetrical

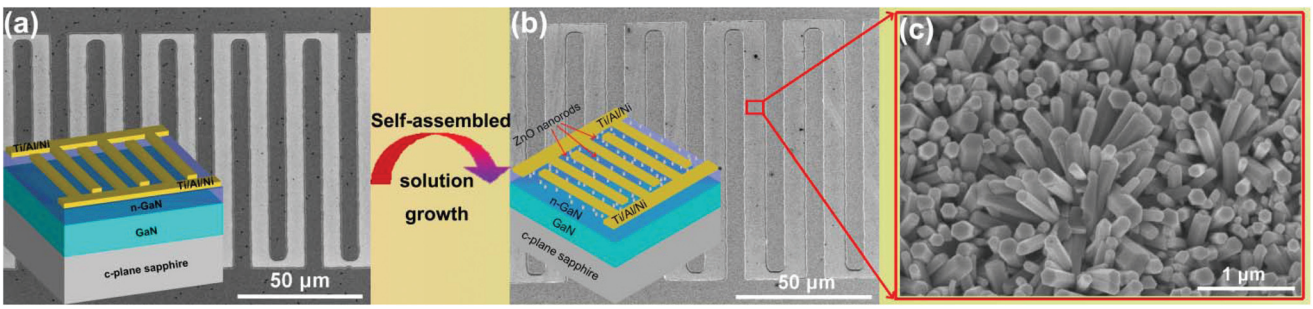

Fig. 1 (a) SEM image of the as-fabricated device. The inset shows the schematic diagram of the GaN-based MSM structure photodetector. (b) SEM image of the physical device after *in situ* assembling the 1D ZnO nanorods. The inset shows the schematic diagram of the 1D ZnO nanorods modified GaN-based MSM structured photodetector. (c) The partial enlarged detail of (b).

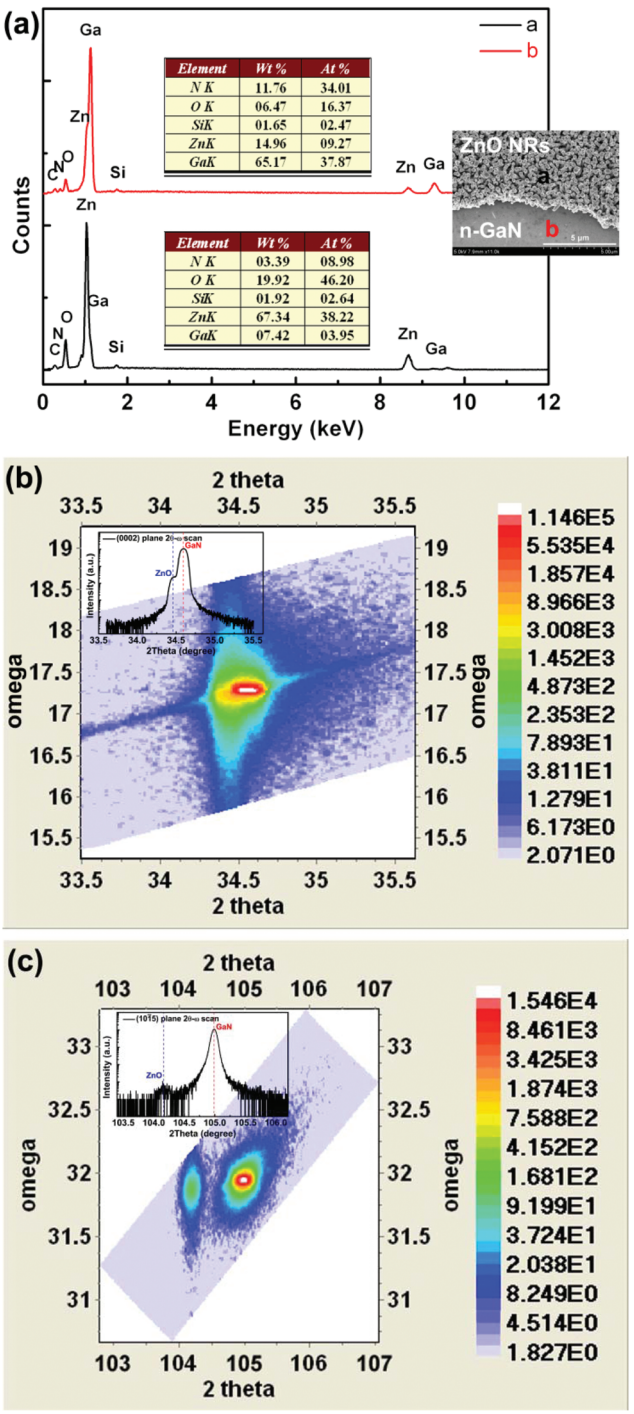

Fig. 2 (a) EDS patterns for the 1D ZnO nanorods/n-GaN heterostructure at different positions. The SEM image indicates the test points. (b) The symmetrical RSM around the (0002) reflection for the 1D ZnO nanorods/n-GaN heterostructure. The inset shows its corresponding 2θ–ω scan result of the (0002) plane. (c) The asymmetrical RSM around the $(10\bar{1}5)$ reflection. The inset shows its corresponding 2θ–ω scan result of the $(10\bar{1}5)$ plane.

reflection, *viz.* (105) plane. The lattice constants for the fully relaxed bulk GaN have been identified as 0.31891 nm and 0.51855 nm for a_0 and c_0, respectively.[33] Thus, the calculated in-plane ($\varepsilon_{\parallel} = (a - a_0)/a_0$) and out-of-plane ($\varepsilon_{\perp} = (c - c_0)/c_0$) strains for the n-GaN epilayer are so small that they can be neglected, which discloses the high crystalline quality of n-GaN epilayer.

In contrast to the n-GaN, there is an additional extended diffuse area in the RLPs of the (0002) reflection for the 1D ZnO nanorods/n-GaN heterostructure, whose peak is located at $2\theta = 34.42°$ (Fig. 2(b)), which corresponds to the (0002) plane peak of the hexagonal structured ZnO, as emphasized in the (0002) plane 2θ–ω scan pattern (inset of Fig. 2(b)). In the asymmetrical RSM around the $(10\bar{1}5)$ reflection (Fig. 2(c)), an additional weak main peak at $2\theta_{(10\bar{1}5)} = 104.16°$ surrounded by colored contour lines is observed. The tilt and the lateral coherence length of the mosaic blocks obviously broaden the RLPs around both the (0002) and $(10\bar{1}5)$ reflections of the 1D ZnO nanorods along the ω-scan direction. Based on eqn (1) and (2), the a and c lattice parameters of the 1D ZnO nanorods are calculated to be 0.3244 nm and 0.52069 nm, respectively. Referring to the lattice constants of fully relaxed hexagonal ZnO nanomaterials ($a_0 = 0.32498$ nm and $c_0 = 0.52066$ nm),[34] it reflects the shrinkage of the in-plane lattice constant a and slight dilatation of the out-of-plane lattice constant c in the self-assembled growth of 1D ZnO nanorods. The related strain $\varepsilon_{\parallel}$ and $\varepsilon_{\perp}$ can be evaluated to be −0.18% and 0.006%, respectively, which indicates that the 1D ZnO nanorods on n-GaN mainly suffer compressive strain in the direction parallel to the surface of n-GaN. In short, the 1D ZnO nanorods/n-GaN heterostructure has good crystalline quality.

The room-temperature PL spectra for the as-grown n-GaN epilayer, 1D ZnO nanorods, and their heterogeneous structural material are presented in Fig. 3. As seen in Fig. 3(a), the PL spectrum of the as-grown n-GaN epilayer exhibits a sharp peak in the vicinity of the band edge at 363 nm (3.41 eV) with a full width at half maximum (FWHM) of 13.5 nm. The so-called yellow-band emission caused by electron recombination between the shallow donor and a deep gap state of donor[35] is also observed. It should be noted that its intensity is very weak. The PL spectrum of 1D ZnO nanorods as measured in Fig. 3(b) shows good multi-peak Gaussian fitting bands centered at around 380 nm (3.26 eV), 388 nm (3.2 eV), and 433 nm (2.86 eV), respectively. Among the three peaks, the one located at 380 nm corresponds to the intense near-band-edge (NBE) emission of ZnO which is attributed to the exciton related recombination. It exhibits a red-shift in comparison with the low-temperature measurement result which is consistent with that reported in literature.[36,37] The peak around 388 nm can be ascribed to the interfacial emission of the 1D ZnO nanorods/n-GaN heterogeneous interface resulting from lattice deformation, due to interference during *in situ* measurements.[38] Additionally, a broad blue emission around 433 nm observed is proved to be the defect related emission from the recombination of the interstitial zinc (Zn_i) with zinc vacancies (V_{Zn}).[39,40] As to the PL spectrum of the 1D ZnO nanorods/n-GaN heterostructure, as shown in Fig. 3(c), it is also well fitted by the multi-peaks Gaussian functions and four

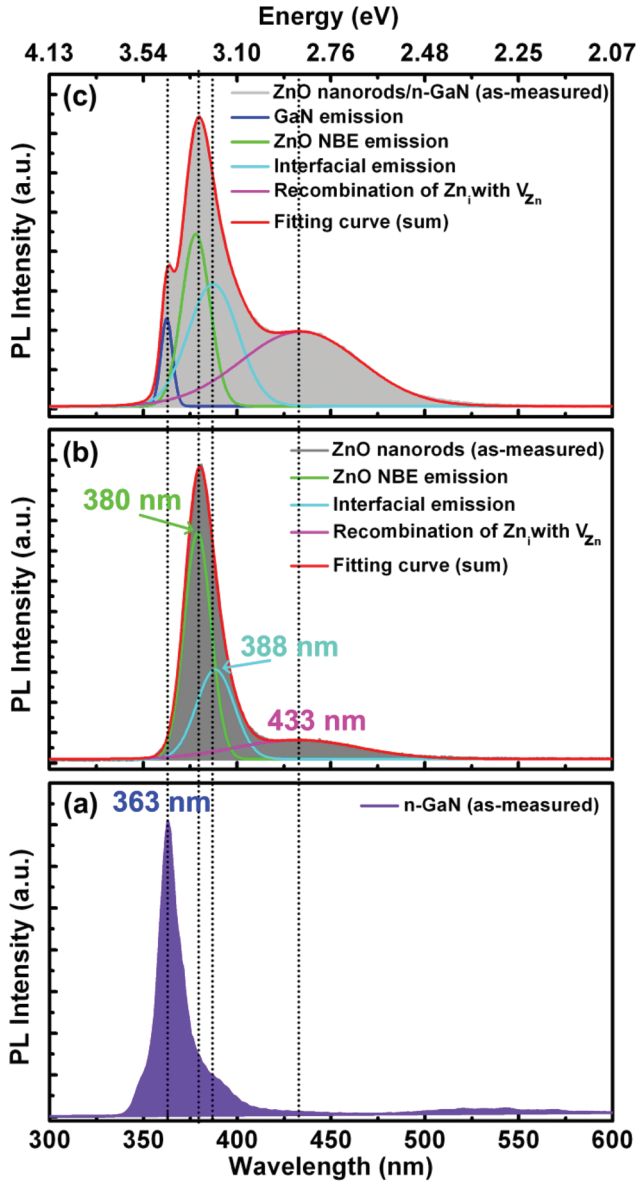

Fig. 3 PL spectra for (a) as-grown n-GaN, (b) 1D ZnO nanorods, and (c) 1D ZnO nanorods/n-GaN heterostructure.

dominant emission peaks are confirmed in accordance with those of the n-GaN and the 1D ZnO nanorods.

To evaluate the photoelectric properties of the 1D ZnO NRs/n-GaN heterogeneous structural material, the MSM structured photodetector was fabricated as described in the Experimental section in detail. Fig. 4(a) shows the *I*–*V* characteristic curves of the device both in dark and under illumination with 367 nm wavelength light, using a semi-logarithmic scale. The inset shows its back-illuminated model. As can be seen, the dark current and the photocurrent for the MSM structure photodetector change linearly with a bias voltage from −5 V to 5 V, which indicates that there is no Schottky barrier in the photodetector. The photocurrent in the photodetector is larger than one order of magnitude than its dark current value. Fig. 4(b) and inset show the spectral responsivities and corresponding EQEs for the 1D ZnO nanorods/n-GaN MSM structured photodetector under different voltage, respectively. The response spectra present bandpass characteristics with a wavelength range between 362 nm and 378 nm. Under 0.1 V bias voltages, the peak responsivity is 0.136 A W^{-1} at 367 nm, corresponding to an EQE of 47.3%. However, the peak responsivity of the photodetector increases rapidly with the increase in the applied bias voltage. Obviously, the peak responsivity increases from 0.136 A W^{-1} under 0.1 V to 0.325 A W^{-1} under 0.3 V, and reaches 0.793 A W^{-1} under 1.3 V that tends to saturation at a certain incident light intensity. The related EQE exceeds 100%, reaching 109.6% under an applied voltage of 0.3 V and is higher than 267.8% under 1.3 V. These results indicate that internal photoelectric gain is possible in the 1D ZnO nanorods/n-GaN MSM structured photodetector and the mechanism involved can be attributed to the photoconductive property of n-GaN photodetector.[41,42]

In general, under the condition of equilibrium excitation, the basic expression of photoconductivity for intrinsic or non-intrinsic semiconductor is given by[43]

$$I_{\mathrm{ph}} = q\eta A\phi_{\mathrm{s}}g \tag{3}$$

where I_{ph} is the dc short circuit photocurrent, η is the quantum efficiency, A is the photosensitive area of the photodetector, q is the charge, ϕ_s is the luminous flux, and g is the internal photoconductive gain. Normally, photoconductivity is a dual carrier (electron and hole) phenomenon. The total photocurrent for electrons and holes can be described as

$$I_{\mathrm{ph}} = \frac{qwt(\Delta n\mu_{\mathrm{e}} + \Delta p\mu_{\mathrm{h}}) \cdot V_{\mathrm{b}}}{l} \tag{4}$$

among them, l and w are respectively on behalf of the length and width of the photosensitive area ($A = lw$), μ_{e} and μ_{h} are the mobility of the electrons and holes, respectively, Δn and Δp are respectively on behalf of the concentration of the photogenerated electrons and holes, t is the time variable, and V_{b} is the applied voltage. For an n-type semiconductor material, its electrical conductivity is mainly determined by the electrons. Therefore, eqn (4) can be simplified as

$$I_{\mathrm{ph}} = \frac{qwt(\Delta n\mu_{\mathrm{e}}) \cdot V_{\mathrm{b}}}{l} \tag{5}$$

Based on eqn (3) and (5), the internal photoconductive gain g can be given by

$$g = \frac{t\Delta n\mu_{\mathrm{e}}V_{\mathrm{b}}}{l^2\eta\phi_{\mathrm{s}}} \tag{6}$$

we assume that the photodetector absorbs the incident light uniformly and completely, the rate equation for the excess electron concentration Δn can be described as

$$\frac{d\Delta n}{d_t} = \frac{\phi_{\mathrm{s}}\eta}{t} - \frac{\Delta n}{\tau} \tag{7}$$

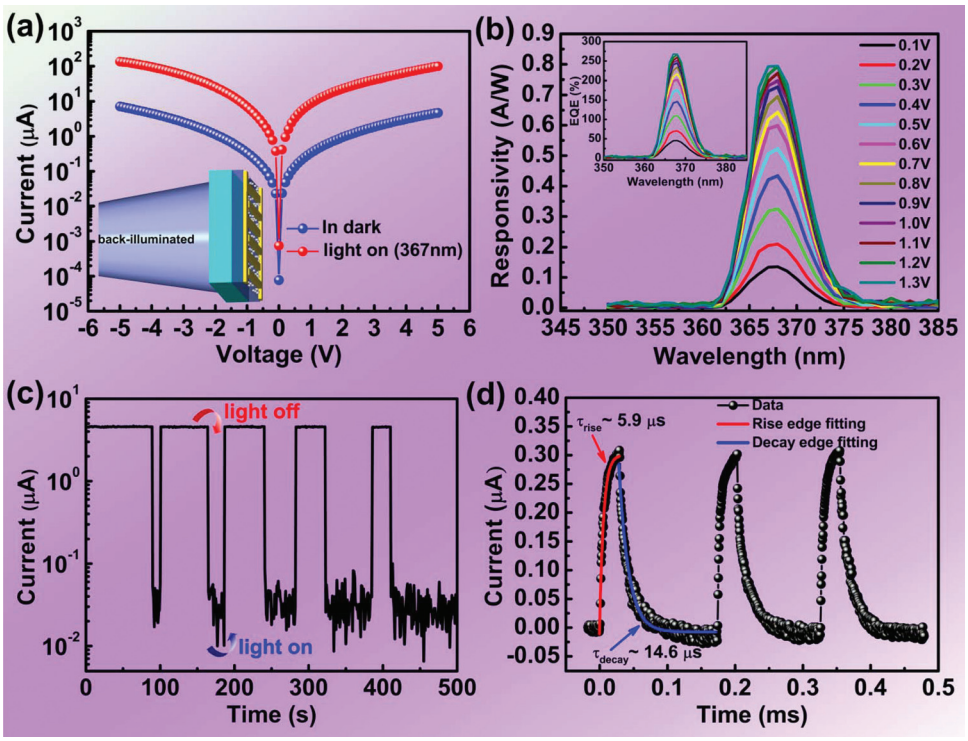

Fig. 4 The *I–V* characteristic curves of the 1D ZnO nanorods/n-GaN MSM structure photodetector in dark and under illumination at 367 nm wavelength light using a semi-logarithmic scale. The inset shows the back-illuminated model. (b) Spectral response characteristics for the 1D ZnO nanorods/n-GaN MSM structured photodetector under different voltages. The inset shows its corresponding EQEs. (c) The time-dependent photocurrent response curve of the 1D ZnO nanorods/n-GaN heterostructure photodetector at 1 V bias voltage when the 367 nm-wavelength illumination alternates switching on and off. (d) The transient spectral response of the 1D ZnO nanorods/n-GaN heterostructure photodetector under 1 V bias voltage.

where τ is the lifetime of the excess carrier. For the steady state, the lifetime can be given by

$$\tau = \frac{\Delta nt}{\eta \phi_s}. \quad (8)$$

Therefore, the internal photoconductive gain g is obtained using eqn (6) and (8) as following

$$g = \frac{\tau V_b \mu_e}{l^2}. \quad (9)$$

Fig. 4(c) shows the time-dependent photocurrent response curve of the 1D ZnO nanorods/n-GaN heterostructure photodetector under 1 V bias voltage, when the incident light alternatively switches on and off. The current when the UV light is on is up to nearly two orders of magnitude larger than that when the UV light is off. This result shows that the conduction of the 1D ZnO nanorods/n-GaN MSM structure photodetector can be greatly enhanced by using UV illumination. In order to evaluate the photoconductive gain g, the transient spectral response of the 1D ZnO nanorods/n-GaN heterostructure photodetector is measured, as shown in Fig. 4(d). A fall time of 14.6 μs at 1 V bias voltage is obtained. As mentioned above, the electron mobility μ_e of n-GaN is measured as 110 $cm^2\ V^{-1}\ s^{-1}$ by Hall measurements. Thus, according to eqn (9), the photoconductivity gain g of the 1D ZnO nanorods/n-GaN MSM structured photodetector can be calculated to be 2.51×10^3 when the interval between the interdigital electrodes is 8 μm.

Based on the 1D ZnO nanorods/n-GaN heterostructure photoconductive detector, a field emission cathode is developed in this paper that effectively combines the ZnO nanorods as emitters with the MSM structured n-GaN photoconductive detector. The photo-assisted enhanced electron transfer from n-GaN to the ZnO can improve the field emission properties of the ZnO nanorod emitters. To evaluate the field emission properties of the 1D ZnO nanorods/n-GaN MSM structured photodetector, a diode configuration is used for the measurement, as shown in Fig. 5(a). The interdigitated electrodes of n-GaN MSM structure photodetector are defined as the cathode electrode (CE) while the ITO glass is used as an anode electrode (AE). The space between CE and AE is fixed at 200 μm by using 200 μm-diameter quartz glass columns. UV light can be incident from the backside of the n-GaN MSM structure photodetector (the side of the sapphire substrate). The typical *J–E* curves of the 1D ZnO nanorods/n-GaN photoconductive detector cathode when the UV light is on and off are presented in Fig. 5(b). The turn-on electric field (E_{TO}) is defined as the electric field when the field emission current density reaches up to 10 μA cm^{-2}.[3,44] Obviously, the E_{TO} for the device in the dark is about 3.6 V μm^{-1} and decreases to 1.36 V μm^{-1} under 367 nm wavelength illumination, and the emission current density

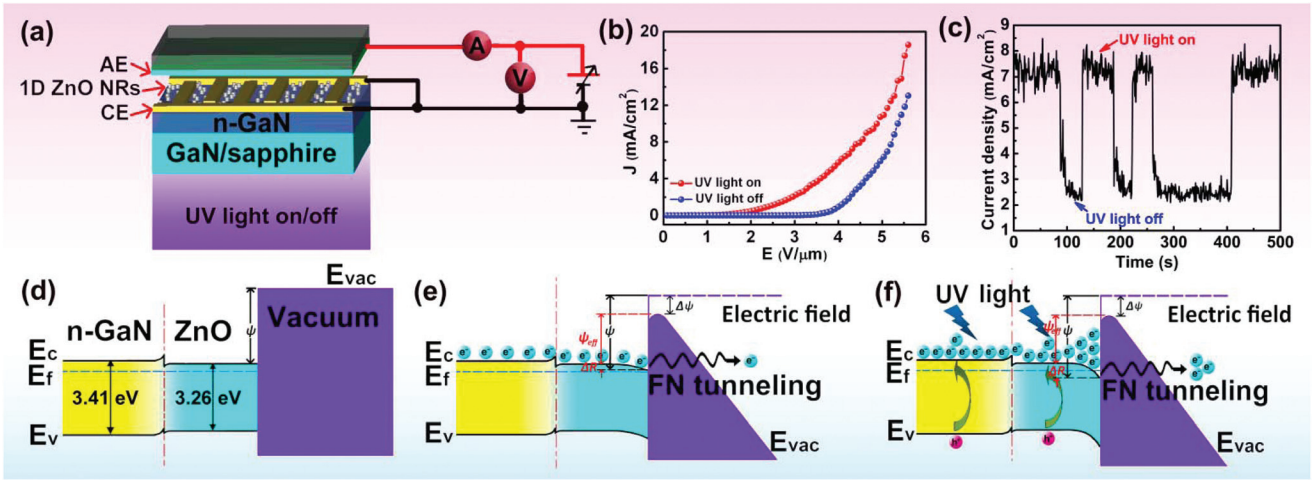

Fig. 5 (a) The schematic diagram of ultraviolet-light-assisted field emission from a 1D ZnO nanorods/n-GaN MSM structure photodetector. (b) The typical *J*–*E* curves of the photodetector when the UV light switches on and off. (c) The time-resolved field emission current density to pulsed UV light. (d)–(f) Schematic energy band diagrams of the 1D ZnO nanorods/n-GaN heterostructure under (d) equilibrium state, (e) field emission in dark and (f) field emission under UV illumination.

J increases from below 3 mA cm^{-2} to as high as 8 mA cm^{-2} at an electric field of 4.5 V μm^{-1}. The time-resolved field emission current density *vs.* pulsed UV light shown in Fig. 5(c), which demonstrates that UV illumination helps decrease the turn-on electric field and increases the emission current of the photoconductive detector cathode.

Generally, the field enhancement factor (β) obtained from the Fowler–Nordheim (F–N) equation is used to evaluate the field emission capability of the nano-emitters. However, it should be noted that the β is mainly related to the geometry, the crystal structure and the distribution density of the nano-emitters, which is not suitable as an evaluation indicator for the same cathode under the externally illuminated and un-illuminated conditions. Therefore, based on the universal field emission equations for semiconductors given by[45]

$$I \approx qn\frac{2\kappa T}{(2m\psi_{\mathrm{eff}})^{1/2}}\cdot\exp\left(-\frac{4\kappa}{3E}{\psi_{\mathrm{eff}}}^{3/2}\right) \quad (10)$$

$$\Psi_{\mathrm{eff}} = \psi - \Delta\psi - \Delta R \quad (11)$$

where n is the carrier concentration of the semiconductor, m is the effective mass of electron, E is the external electric field, κ is the Boltzmann's constant, T is the absolute temperature, ψ and $\Delta\psi$ are the potential energy of the electrons in the conduction band and its variation under the applied electric field, ΔR represents the change of the conduction band due to band bending, and ψ_{eff} is the effective potential energy of the electrons in the conduction band. The decrease of E_{TO} and the increase of the field emission current density should be ascribed to the reduction of the effective potential barrier height due to the electric field induced band bending ($\Delta\psi$) and the conduction band bending (ΔR) of ZnO caused by electron activation and accumulation at the surface under UV illumination. This statement can be explained on the basis of the energy band diagram and electric field theory. As shown in Fig. 5(d), the band gaps of n-GaN and ZnO are measured to be 3.41 eV and 3.26 eV by the PL spectra (Fig. 3), respectively. The electron affinities (χ) for GaN and ZnO are confirmed to be 4.2 eV and 4.35 eV.[46] Without UV illumination, under an equilibrium state, the n-GaN and ZnO establish equilibrium with a consistent Fermi energy level (E_{f}). Due to the small band offset between them, when a strong electric field is applied to the device, the electrons move from the conduction band (E_{c}) of n-GaN to that of ZnO nanorods and accumulate in the E_{c} of the ZnO nanorod tips, resulting in the E_{c} of ZnO nanorods tilting toward the E_{f}, and the variation is described as ΔR. Meanwhile, the vacuum energy level (E_{vac}) slopes down gradually with the increase of the applied electric field, forming a triangular barrier, and the potential energy under the electric field is reduced as $\Delta\psi$. The conduction band electrons of the ZnO nanorods thus tunnel through the triangular barrier to form a field emission current under the strong electric field, as shown in Fig. 5(e). By comparison, when a 1D ZnO nanorods/n-GaN photoconductive detector cathode is exposed to UV light, on the one hand, the incident photons ($h\nu \geq E_{\mathrm{g}}$) absorbed by the photoconductive detector will excite the electrons of valence band (E_{v}) to the E_{c}, which supply a large number of additional electrons to both conduction bands. On the other hand, the electrons in the conduction bands will accumulate in the E_{c} of the ZnO nanorod tips under the applied electric field, resulting in increased tilting of E_{c} towards E_{f}, which means an increase of ΔR, as shown in Fig. 5(f). Based on eqn (11), the result is equivalent to the reduction of the effective potential barrier height (ψ_{eff}), which is beneficial for increased electron tunneling to contribute to the field emission current. Thus, the improved field emission behaviors of the 1D ZnO nanorods/n-GaN heterostructure photoconductive detector by UV light can be ascribed to the

increased electron concentration in the conduction band and the reduction of effective potential barrier height (ψ_{eff}).

Conclusions

In this paper, an n-GaN MSM structure photodetector is assembled with 1D ZnO nanorods by a self-assembled hydrothermal growth method. The 1D ZnO nanorods/n-GaN heterogeneous structural device integrates the functions of photoelectric detection and electron emission, which can be developed as a high-efficiency UV-light-assisted enhanced field emission electron source. The optical, photoelectric, and field emission properties are investigated in detail. The results show that the 1D ZnO nanorods/n-GaN heterostructure photodetector presents photoconductive characteristics that has a peak spectral responsivity of 0.793 A W^{-1} at 1.3 V, corresponding to an EQE higher than 267.8%, with an internal photoconductive gain reaching up to 2.51×10^3. Its E_{TO} of field emission can be greatly reduced from 3.6 V μm^{-1} in the dark to 1.36 V μm^{-1} under 367 nm wavelength illumination, and the J increases from below 3 mA cm^{-2} to as high as 8 mA cm^{-2} at an electric field of 4.5 V μm^{-1}. The improved field emission performances under UV illumination can be attributed to the increase of the electron concentration in the conduction band and the reduction of the effective potential barrier height in the ZnO nanorods. This research shows promise for carrying out an optical field positive-feedback process in field emission EB pumped AlGaN-based UV light sources that can also be generalized for the fabrication of DUV light sources.

Conflicts of interest

The authors declare no financial competing interests.

Acknowledgements

This work was partially supported by the National Natural Science Foundation of China (Grant No. 61504144 and 51472230), and the Jilin Provincial Science & Technology Department (Grant No. 20170520156JH).

References

1 T. Oto, R. G. Banal, K. Kataoka, M. Funato and Y. Kawakami, *Nat. Photonics*, 2010, **4**, 767–770.
2 F. Tabataba-Vakili, T. Wunderer, M. Kneissl, Z. Yang, M. Teepe, M. Batres, M. Feneberg, B. Vancil and N. M. Johnson, *Appl. Phys. Lett.*, 2016, **109**, 181105.
3 Y. Chen, L. Hu, H. Song, H. Jiang, D. Li, G. Miao, Z. Li, X. Sun, Z. Zhang and T. Guo, *Nanoscale*, 2014, **6**, 13544–13549.
4 J.-W. Jeong, J.-W. Kim, J.-T. Kang, S. Choi, S. Ahn and Y.-H. Song, *Nanotechnology*, 2013, **24**, 085201.
5 K. B. K. Teo, E. Minoux, L. Hudanski, F. Peauger, J.-P. Schnell, L. Gangloff, P. Legagneux, D. Dieumegard, G. A. J. Amaratunga and W. I. Milne, *Nature*, 2005, **437**, 968.
6 G. Ulisse, F. Brunetti and A. D. Carlo, *IEEE Trans. Electron Devices*, 2011, **58**, 3200–3204.
7 Z. L. Wang, *Mater. Today*, 2004, **7**, 26–33.
8 L. Schmidt-Mende and J. L. MacManus-Driscoll, *Mater. Today*, 2007, **10**, 40–48.
9 P. K. Shrestha, Y. T. Chun and D. Chu, *Light: Sci. Appl.*, 2015, **4**, e259.
10 J.-T. Yan, C.-H. Chen, S.-F. Yen and C.-T. Lee, *IEEE Photonics Technol. Lett.*, 2010, **22**, 146–148.
11 G. C. Park, S. M. Hwang, S. M. Lee, J. H. Choi, K. M. Song, H. Y. Kim, H.-S. Kim, S.-J. Eum, S.-B. Jung, J. H. Lim and J. Joo, *Sci. Rep.*, 2015, **5**, 10410.
12 Y. F. Hsu, Y. Y. Xi, A. B. Djurišić and W. K. Chan, *Appl. Phys. Lett.*, 2008, **92**, 133507.
13 J. Tian, E. Uchaker, Q. Zhang and G. Cao, *ACS Appl. Mater. Interfaces*, 2014, **6**, 4466–4472.
14 H. Zhou, M. Wissinger, J. Fallert, R. Hauschild, F. Stelzl, C. Klingshirn and H. Kalt, *Appl. Phys. Lett.*, 2007, **91**, 181112.
15 J. Dai, C. X. Xu and X. W. Sun, *Adv. Mater.*, 2011, **23**, 4115–4119.
16 S. Thiemann, M. Gruber, I. Lokteva, J. Hirschmann, M. Halik and J. Zaumseil, *ACS Appl. Mater. Interfaces*, 2013, **5**, 1656–1662.
17 Y. H. Liu, S.-J. Young, C. H. Hsiao, L.-W. Ji, T. H. Meen, W. Water and S.-J. Chang, *IEEE Photonics Technol. Lett.*, 2014, **26**, 645–648.
18 H. Zhou, P. Gui, Q. Yu, J. Mei, H. Wang and G. Fang, *J. Mater. Chem. C*, 2015, **3**, 990–994.
19 V. Q. Dang, T. Q. Trung, D. Kim, L. T. Duy, B.-U. Hwang, D.-W. Lee, B.-Y. Kim, L. D. Toan and N.-E. Lee, *Small*, 2015, **11**, 3054–3065.
20 S. Tian, F. Yang, D. Zeng and C. Xie, *J. Phys. Chem. C*, 2012, **116**, 10586–10591.
21 Z. Zhang, G. W. Meng, Q. Wu, Z. Hu, J. K. Chen, Q. L. Xu and F. Zhou, *Sci. Rep.*, 2014, **4**, 4676.
22 G. J. Wang, Z. C. Li, M. Y. Li, J. C. Liao, C. H. Chen, S. S. Lv and C. Q. Shi, *Phys. Chem. Chem. Phys.*, 2015, **17**, 31822–31829.
23 C. C. Yang, Y. K. Su, M. Y. Chuang, H. C. Yu and C. H. Hsiao, *IEEE Trans. Electron Devices*, 2015, **62**, 2300–2305.
24 Z. H. Wang, C. C. Yang, H. C. Yu, H. T. Yeh, Y. M. Peng and Y. K. Su, *IEEE Trans. Electron Devices*, 2018, **65**, 251–256.
25 C. Park, J. Lee, H.-M. So and W. S. Chang, *J. Mater. Chem. C*, 2015, **3**, 2737–2743.
26 Y. R. Chen, Z. W. Zhang, Z. M. Li, H. Jiang, G. Q. Miao and H. Song, *Phys. Status Solidi A*, 2018, **215**, 1700358.
27 Y. Chen, H. Jiang, D. Li, H. Song, Z. Li, X. Sun, G. Miao and H. Zhao, *Nanoscale Res. Lett.*, 2011, **6**, 537.
28 R. Chierchia, T. Böttcher, H. Heinke, S. Einfeldt, S. Figge and D. Hommel, *J. Appl. Phys.*, 2003, **93**, 8918–8925.

29 M. A. Moram and M. E. Vickers, *Rep. Prog. Phys.*, 2009, **72**, 036502.
30 A. V. Kuchuk, H. V. Stanchu, C. Li, M. E. Ware, Yu. I. Mazur, V. P. Kladko, A. E. Belyaev and G. J. Salamo, *J. Appl. Phys.*, 2014, **116**, 224302.
31 H. Kröncke, S. Figge, T. Aschenbrenner and D. Hommel, *J. Cryst. Growth*, 2013, **381**, 100–106.
32 H. Liu, S. Chu, R. Peng, M. Liu, Z. Chen, B. Jin and S. Chu, *CrystEngComm*, 2015, **17**, 4818–4824.
33 M. Yamaguchi, T. Yagi, T. Sota, T. Deguchi, K. Shimada and S. Nakamura, *J. Appl. Phys.*, 1999, **85**, 8502–8504.
34 Z. W. Pan, Z. R. Dai and Z. L. Wang, *Science*, 2001, **291**, 1947–1949.
35 T. Suski, P. Perlin, H. Teisseyre, M. Leszczyński, I. Grzegory, J. Jun, M. Boćkowshi and S. Porowski, *Appl. Phys. Lett.*, 1998, **67**, 2188–2190.
36 Y. Chen, D. Bagnall and T. Yao, *Mater. Sci. Eng., B*, 2000, **75**, 190–198.
37 J. H. Kim, E. M. Kim, D. Andeen, D. Thomson, S. P. DenBaars and F. F. Lange, *Adv. Funct. Mater.*, 2007, **17**, 463–471.
38 A. J. Chen, X. M. Wu, Z. D. Sha, L. J. Zhuge and Y. D. Meng, *J. Phys. D: Appl. Phys.*, 2006, **39**, 4762–4765.
39 H. Zeng, G. Duan, Y. Li, S. Yang, X. Xu and W. Cai, *Adv. Funct. Mater.*, 2010, **20**, 561–572.
40 C. Park, J. Lee and W. S. Chang, *J. Phys. Chem. C*, 2015, **119**, 16984–16990.
41 P. Kung, X. Zhang, D. Waller, A. Saxler, J. Piotrowski and A. Rogalski, *Appl. Phys. Lett.*, 1995, **67**, 3792–3794.
42 E. Muñoz, E. Monroy, J. A. Garrido, I. Izpura, F. J. Sánchez, M. A. Sánchez-García and E. Calleja, *Appl. Phys. Lett.*, 1997, **71**, 870–872.
43 S. Han, Z. Zhang, J. Zhang, L. Wang, J. Zheng, H. Zhao, Y. Zhang, M. Jiang, S. Wang, D. Zhao, C. Shan, B. Li and D. Shen, *Appl. Phys. Lett.*, 2011, **99**, 242105.
44 C. Wu, T. W. Kim, T. Guo and F. Li, *Sci. Rep.*, 2016, **6**, 38613.
45 R. Stratton, *Proc. Phys. Soc., London, Sect. B*, 1955, **68**, 746–757.
46 O. Lupan, T. Pauporté and B. Viana, *Adv. Mater.*, 2010, **22**, 3298–3302.